Journal of Materials Research and Technology 43 (2026) 2220–2232

Contents lists available at ScienceDirect

Journal of Materials Research and Technology

journal homepage: www.elsevier.com/locate/jmrt

Process-controlled crystallinity in PA12 produced by Multi Jet Fusion and hot pressing: Tailoring cooling profiles to enhance fatigue resistance

Raffaele De Biasi [a,b,*], Damiano Foltran [b], Giulia Fredi [b,c], Matteo Perini [d], Filippo Berto [a], Matteo Benedetti [b,**]

[a] Department of Chemical Engineering Materials Environment, Sapienza University of Rome, Via Eudossiana 18, 00184, Roma, Italy
[b] Department of Industrial Engineering, University of Trento, Via Sommarive 9, Trento, 38123, Italy
[c] National Interuniversity Consortium of Materials Science and Technology (INSTM), 50121, Florence, Italy
[d] ProM Facility, Via Fortunato Zeni 8, Rovereto, 38068, Italy

ARTICLE INFO

Keywords:
Multi Jet Fusion (MJF)
Hot press
Polyamide 12
PA12
Fatigue

ABSTRACT

This work investigates the role of manufacturing-induced crystallinity on the fatigue behavior of Polyamide 12 (PA12), with particular emphasis on the role of temperature in fatigue performance. Specimens produced by Multi Jet Fusion (MJF) are compared with hot-pressed (HP) counterparts manufactured from the same powder batch under controlled cooling conditions. An extended cooling (EC) protocol is introduced to tailor crystallinity by prolonging the residence time within the crystallization window. Comprehensive thermal, microstructural, and mechanical characterization is combined with fatigue testing and in-situ infrared thermography. Results show that higher crystallinity significantly reduces viscoelastic dissipation and self-heating, leading to improved fatigue resistance. Despite lower defect content, standard HP specimens exhibit inferior fatigue performance compared to MJF due to reduced crystallinity. The EC protocol effectively bridges this gap, enhancing fatigue life and matching the MJF fatigue performance. Based on these findings, optimized cooling parameters are proposed and experimentally validated, demonstrating that crystallinity control is an effective process-level strategy to improve the fatigue performance of PA12.

1. Introduction

Polyamide 12 (PA12) is the best-established polymer feedstock for powder bed fusion (PBF) processes, and it serves as the benchmark material in both industrial applications and academic research [1]. Its diffused adoption is based on an interesting combination of properties: low moisture absorption, good chemical resistance, broad sintering window, and competitive mechanical performance with other engineering thermoplastics [2–6]. Among PBF technologies, Multi Jet Fusion (MJF) has emerged as an industrially relevant variant that addresses some of the throughput and repeatability limitations of other PBF techniques such as selective laser sintering (SLS) [7,8]. MJF, which relies on a fusing agent selectively deposited onto the powder bed and promoting powder fusion when activated by an infrared lamp, enables higher production rates and improved powder recyclability compared to SLS, while offering comparable dimensional accuracy and improved surface uniformity [9]. These advantages, combined with the maturity of PA12 as a material, have driven the progressive adoption of MJF-printed components in high-end applications in the automotive, aerospace, and medical device sectors. In all these contexts, components are routinely subjected to repeated mechanical loading, and the question of long-term mechanical reliability under cyclic conditions becomes central. Understanding and controlling the fatigue performance of PA12 is therefore not just a material science concern but, fundamentally, a manufacturing process question.

Fatigue failure is among the dominant failure modes for structural components in service. For polymeric components, this issue is worsened by viscoelastic dissipation: a fraction of the mechanical energy input per cycle is converted into heat, generating a temperature rise within the specimen that can approach or exceed the glass transition temperature (T_g). In PA12, with T_g near 40–50 °C [5], this thermal-fatigue coupling is especially relevant. As temperature rises, the storage modulus decreases, the viscoelastic damping increases, and self-heating accelerates, thereby promoting further softening and

* Corresponding author. Department of Chemical Engineering Materials Environment, Sapienza University of Rome, Via Eudossiana 18, 00184, Roma, Italy.
** Corresponding author.
E-mail addresses: raffaele.debiasi@uniroma1.it (R. De Biasi), matteo.benedetti@unitn.it (M. Benedetti).

https://doi.org/10.1016/j.jmrt.2026.06.196
Received 20 May 2026; Received in revised form 19 June 2026; Accepted 20 June 2026
Available online 21 June 2026
2238-7854/© 2026 The Authors. Published by Elsevier B.V. This is an open access article under the CC BY license (http://creativecommons.org/licenses/by/4.0/).

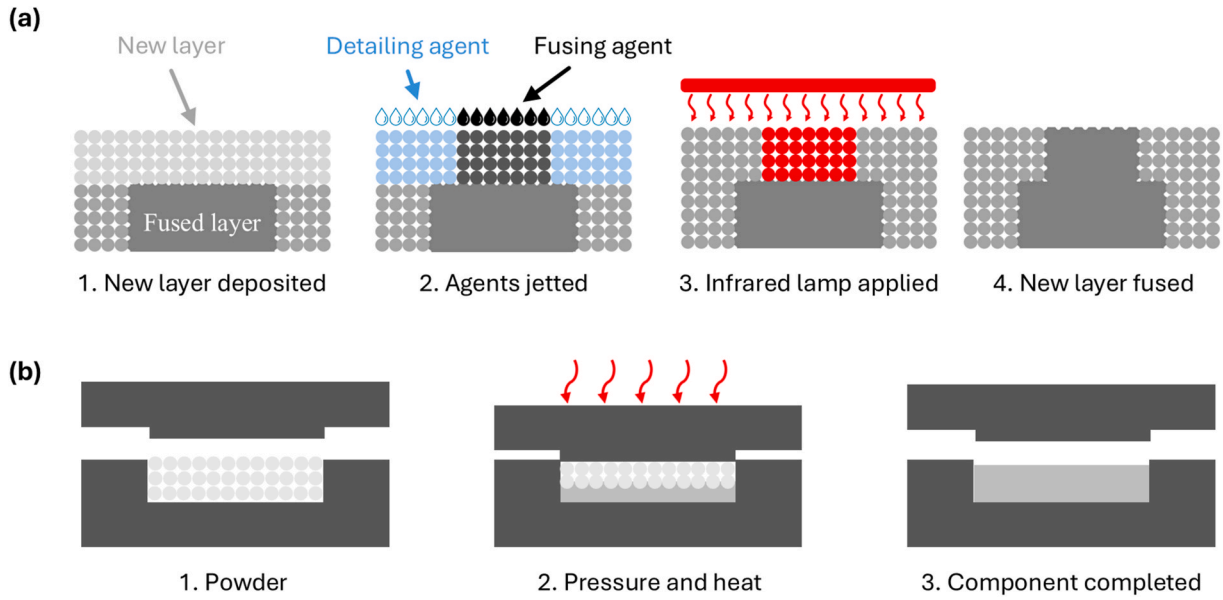

Fig. 1. Schematic representation of the MJF (a) – adapted from Ref. [22] – and hot press (HP) manufacturing process (b).

premature failure [10–13]. Since glass transition involves only the amorphous phase, the severity of the described mechanism is governed by the material's degree of crystallinity (χ_c). Increasing χ_c reduces the fraction of material undergoing the glass transition and introduces crystalline constraints that limit amorphous chain mobility, which likely decreases heat generation under cyclic loading [14]. Despite the relevance of these mechanisms, the literature has only focused on the influence of build orientation and porosity on S–N behavior for MJF PA12 [15], while the role of testing frequency, thermal-fatigue coupling, and the effect of manufacturing-induced crystallinity on fatigue response have received limited attention so far.

The crystallinity of a semicrystalline polymer depends on the thermal history imposed during processing, and especially on the cooling rate from the melt. Crystalline domains nucleate and grow as the polymer melt cools through the crystallization temperature window, with the available time for this process directly governing the resulting χ_c, crystal size, and distribution of polymorphs [14]. In PA12, slow cooling from the melt leads to a high χ_c and the formation of the γ phase with parallel chain arrangement, while faster cooling yields the γ' phase and/or reduces χ_c [16]. This is also true for PBF processing, with slower cooling and prolonged persistence in the crystallization window resulting in high χ_c and larger spherulites [17,18]. Specifically, for MJF, it was shown that build position within the MJF chamber, and the associated local cooling rate, directly translates into spatial gradients of crystallinity and mechanical performance [19]. Moreover, the effective cooling rate is considerably lower than in most conventional manufacturing routes: after printing, the build unit is transferred to a dedicated processing station where the as-printed parts remain surrounded by the hot powder bed in the so-called “natural cooling”. This slow, passive cooling, conducted at temperatures very close to the onset T_m, provides extensive time within the crystallization window and is the primary reason why MJF PA12 typically exhibits higher crystallinity than conventionally processed material [20,21]. Controlling the cooling profile therefore represents a direct lever on the microstructure of PA12 components, and hence on their fatigue resistance. Thus, crystallinity can be treated as a process-controlled parameter, motivating the development of a predictive framework to guide process design.

A processing route in which this lever can be operated with full experimental control is hot pressing (HP). In this process, PA12 powder is consolidated through applied pressure at a temperature above the material's T_m, producing dense, pore-free plates from which specimens can be machined or cut. Unlike MJF, HP allows independent and precise control of temperature, pressure, and cooling rate, making it suitable for isolating the effect of thermal history on material microstructure and properties. A comparative graphical representation of the manufacturing techniques is provided in Fig. 1. Despite this potential, HP has been rarely employed as a direct comparator to MJF in the literature, and, to the best of the authors' knowledge, no study has produced both HP and MJF specimens from the same powder batch while systematically varying the HP cooling profile. This aspect carries both scientific and industrial significance. In industrial MJF operations, the standard powder refresh ratio of 20% virgin to 80% recycled material means that the feedstock used for printing is a blend of powders with different thermal histories, including exposure to temperatures near T_m for cumulative periods of tens of hours. Whether this powder can be processed through an alternative route such as HP, and with which resulting properties, is a question relevant also for circular economy considerations, as HP can be a relevant processing route to safely handle and recycle polymer powder when it is no longer useable for MJF.

In the present work, MJF specimens are compared to HP specimens produced from powder recovered from the MJF chamber, thereby ensuring a controlled and industrially representative comparison. Furthermore, the HP route is used to introduce an extended cooling (EC) protocol: a stepwise cooling process designed to increase the time the material spends within the crystallization window (approx. 180–80 °C) by reducing the cooling rate to 0.5 °C/min in this interval. This protocol positions HP not merely as a conventional manufacturing benchmark but as a process-based strategy for producing PA12 components with targeted crystallinity, thereby enabling a direct investigation of the microstructure–fatigue relationship.

Hence, the aim of this work is to understand how manufacturing-induced crystallinity affects fatigue resistance of PA12 and if an extended cooling HP protocol can bridge the crystallinity gap with MJF and HP specimens, thus controlling self-heating and extending the fatigue life. Although the relationship between crystallinity and fatigue performance has already been investigated on PA12 [23,24], in those works the crystallinity differences was an uncontrolled consequence of the investigated processes (injection molding and selective laser sintering). Conversely, the novelty of this work is the use of the HP process with a deliberately engineered cooling protocol to isolate and tune crystallinity, while simultaneously quantifying the associated

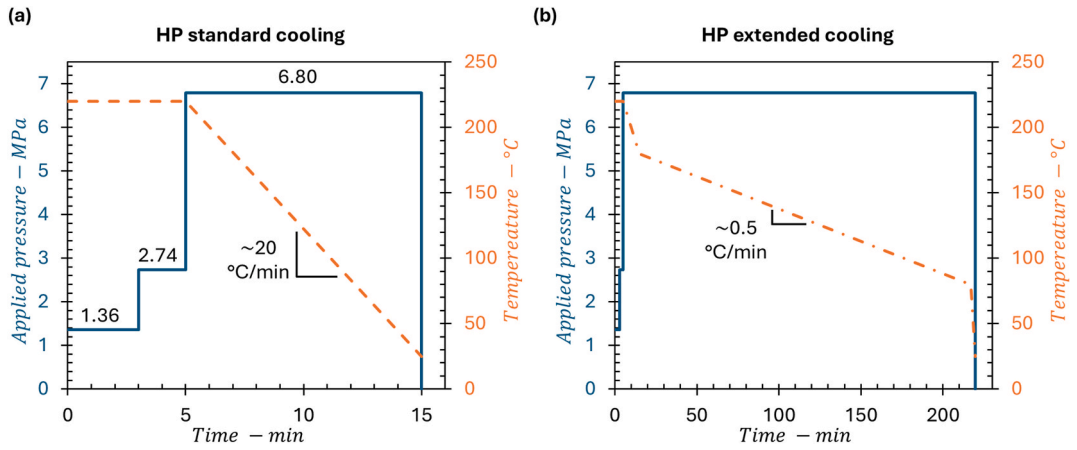

Fig. 2. Temperature and applied pressure profile in the hot pressing (HP) standard (a) and extended cooling (b) process. The two procedures share the same temperature and pressure profile to reach PA12 melting point.

self-heating via IR thermography to clearly highlight the role of crystallinity in enhancing the fatigue performance.

The work reports a comprehensive experimental comparison of PA12 specimens manufactured by MJF and by HP (with standard and extended cooling protocols), produced from the same powder batch. Characterization includes Fourier-transform infrared spectroscopy (FT-IR), differential scanning calorimetry (DSC), thermogravimetric analysis (TGA), dynamic mechanical thermal analysis (DMTA), and X-ray computed tomography (CT), providing a complete overview of the chemical, microstructural, and thermal state of each sample. These results are then correlated with those of quasi-static tensile tests and fatigue tests at R = 0.1 are performed, complemented by in-situ infrared thermography to quantify self-heating during cyclic loading. Once the relationship between crystallinity and fatigue is established, a process-oriented framework is developed to guide the selection of cooling parameters for targeted crystallinity control, and its effectiveness is evaluated through experimental validation.

2. Materials and methods

2.1. Specimen design and manufacturing

In this work, the mechanical properties of PA12 manufactured through Additive Manufacturing (AM) Multi Jet Fusion (MJF) and hot pressing (HP) are compared. The material selected is PA12 powder, commercially known as HP 3D reusability PA12, and to increase the industrial relevance of the work, the powder is a mixture of virgin (20%) and MJF-recycled (80%) powder, as typical for the AM process.

For the MJF specimens, the employed equipment is an HP Multi Jet Fusion 4200 printer, and the specimens' printing orientation is fixed at 30° with respect to both the x and y axes of the building plate. Specimens are realized using the "balanced" settings suggested by the machine

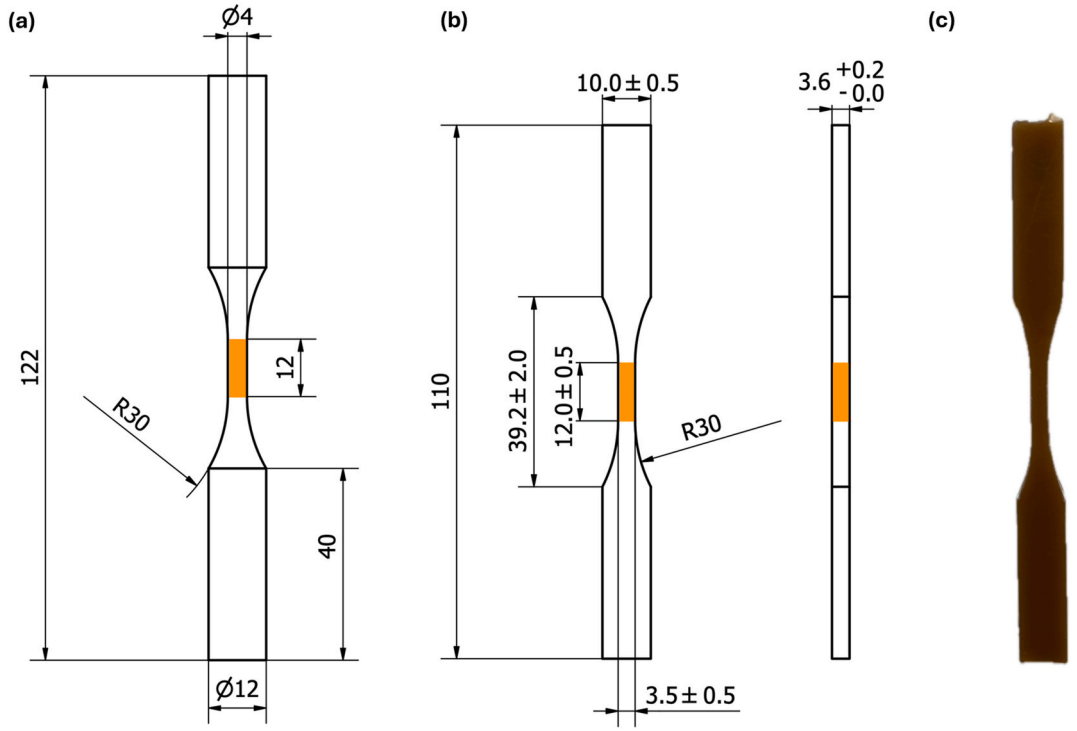

Fig. 3. Comparison of the specimens' geometry for fatigue testing. Gauge length volume between (a) MJF and (b) HP geometry is designed to match. (c) HP specimen obtained from the plate after laser cutting.

manufacturer. For the HP specimens, the manufacturing is composed of two steps: hot pressing is used to produce plates that are laser cut. Initially, the PA12 powder is dried in an oven for 72-96 h at 60 °C, then the powder is hot pressed in a Carver hydraulic press, model 4122. The manufactured plates, with final dimensions 120 x 120 × 3.6 mm^3, are then laser cut to the geometries needed for the subsequent characterization.

As is well known, the melting and cooling processes of PA12 play a crucial role in determining the properties of the final component; in particular, the cooling rate has a direct influence on the resulting degree of crystallinity [10,25]. In the MJF process, the cooling rate of the components is dictated by the post-processing station, where the printing chamber is left in "natural cooling" till room temperature.

In contrast, in the HP process the cooling phase can be completely tailored, and two profiles are analyzed. Fig. 2(a) depicts the pressure and the temperature profile of the standard manufacturing process, while Fig. 2(b) presents the temperature profile for extended cooling, a processing technique able to increase the crystallinity in the PA12 specimens. In both configurations, the pressure is applied stepwise, while the temperature is kept constant to 220 °C in the initial process phase, when the powder is melted. Cooling is performed at constant 20 °C/min for the standard process, while it is divided into three steps in the extended one: (i) 20 °C/min down to 180 °C, where crystallization begins; (ii) 0.5 °C/min down to 80 °C below which further crystallization is negligible; (iii) 20 °C/min to room temperature. This stepwise process maximizes the time spent in the 180-80 °C temperature window, while reducing the overall manufacturing time.

To measure the impact of the manufacturing process on the PA12 mechanical properties, different specimens' geometries are realized. For tensile testing, 1BA specimens are realized in MJF and HP according to the UNI EN ISO 527 standard. For dynamic mechanical thermal analysis (DMTA) testing, rectangular specimens 35 mm long, 10 mm wide and 3.6 mm thick were obtained by HP and MJF.

For fatigue testing, the geometry of the specimens realized with the MJF technology is round and coherent with [22], as represented in Fig. 3 (a). The geometry of the specimens produced via HP is similar but characterized by a rectangular cross-section, due to the inherent challenges of producing a specimen with circular cross section via this technique. Specimen dimensions are selected to ensure that the volume of material within the gauge length matches that of the MJF specimen. This is specifically set to limit the influence of the statistical size effect on fatigue phenomena, whereby a larger material volume increases the likelihood of hosting critical defects acting as crack initiation sites [26]. A detailed representation of the specimens' geometry is provided in Fig. 3(b), while a picture of an HP specimen is presented in Fig. 3(c).

2.2. Specimen and powder characterization

Base material and the specimens obtained after the manufacturing processes undergo complete Fourier transform infrared (FT-IR) spectroscopy and thermal analyses to fully characterize the impact of the manufacturing process on the material.

PA12 powder and specimens manufactured via MJF and standard HP are analyzed with the FT-IR using a PerkinElmer Spectrum One spectrometer (Waltham, USA). The analyses are performed in the spectral range 4000–650 cm^{-1}, with 100 scans acquired per spectrum at a resolution of 4 cm^{-1}. The aim is to investigate possible signs of degradation or oxidative phenomena in the powder and to evaluate whether the processing routes induced chemical modifications in the bulk material.

Thermal analyses investigate the behavior of PA12 in its different forms (powder, MJF, and HP). Each technique provided complementary information: Differential scanning calorimetry (DSC) is used to evaluate crystallinity (χ_c), glass transition temperature (T_g) and melting temperature (T_m); Thermogravimetric analysis (TGA) is performed to assess thermal stability and degradation behavior, aspects particularly relevant for defining the hot-pressing parameters; and DMTA is carried out to characterize the viscoelastic response of PA12 as a function of temperature and frequency.

Table 1
Set-up parameters for the CT three-dimensional geometrical reconstruction.

Voltage – kV	Current - μA	Voxel size - μm	Cu physical filter – mm	Nr. Projections
200	242	39.09	0.5	2050

DSC measurements are performed on powder, MJF, standard HP, and extended cooling HP samples. Approximately 10–12 mg of material is analyzed using a Mettler Toledo DSC 5+ machine, with heating and cooling rates of 10 °C/min in the temperature range 0–220 °C with controlled atmosphere given by a nitrogen flux equal to 100 ml/min. Each measurement consists of a heating–cooling–heating cycle and the degree of crystallinity is calculated according to Equation (1):

$$\chi_c = \frac{\Delta H_m - \Delta H_{cc}}{\Delta H_m^0} \times 100 \quad (1)$$

where ΔH_m is the measured melting enthalpy of the polymer during the first heating scan, ΔH_{cc} is the cold crystallization enthalpy, and ΔH_m^0 is the melting enthalpy of a fully crystalline PA12 set at 209.3 J/g [27–29].

TGA is performed on PA12 powder to identify the maximum processing temperature for hot pressing. The tests are carried out under two different atmospheres, air and nitrogen with gas flow of 100 ml/min, in the temperature range of 0–700 °C with a heating rate of 10 °C/min. Approximately 20-25 mg of material are analyzed using a Mettler Toledo TG50 instrument.

DMTA is performed using a TA Instruments DMA Q800 on standard HP and MJF specimens using the single cantilever configuration, with a distance between the grips fixed at 17.5 mm. The starting tests' temperature is −30 °C and the end temperature is 120 °C with a heating rate of 3 °C/min, the imposed displacement amplitude was 20 μm applied at a frequency of 1 Hz.

A metrological analysis is also performed on standard HP specimens to characterize the manufacturing quality. One of the fatigue specimens is randomly selected to undergo complete three-dimensional Computer Tomography (CT)-based geometrical reconstruction. The equipment employed is a Zeiss Metrotom, using the values of the parameters listed in Table 1. The three-dimensional reconstruction and porosity quantification are performed using the ORS-Dragonfly image analysis software (Comet Technologies Canada Inc., Canada).

2.3. Quasi-static and fatigue testing

Quasi-static tensile tests are performed in agreement with UNI EN ISO 527 standard, using an electromechanical testing machine Instron 5969 equipped with a 10 kN load cell and an Instron 2620-601 dynamic extensometer. The test speed is set to 1 mm/min. Five standard HP specimens are tested until failure. Elastic modulus is computed as the slope of the stress-extensometer strain curve between the strain levels of 0.05% and 0.25%, while the yield strength (σ_y) is calculated as the first local maximum, and the stress and strain at break (σ_b, ε_b) are calculated in correspondence of the specimen failure.

Fatigue tests were carried out with an electrodynamic testing machine StepLab UDO20 equipped with a 20 kN load cell. Two distinct sets of tests are conducted for each material to evaluate the effect of testing frequency on the fatigue response. In agreement with [15,30,31], the frequencies are set equal to 5Hz and 3Hz. Tests are performed with stress ratio set to R = 0.1 to avoid compressive loads that could induce undesired buckling phenomena. Each test is terminated upon reaching the run-out condition at 10^6 cycles, complete specimen failure, or excessive plasticization driven by thermal effects. In the latter case, the test is stopped when the imposed displacement exceeds 4 mm; under this

Table 2
PA12 characterization parameter sets as per [34–37].

n - #	U - J/mol	$K_G - K^2$	$K_0 - s^{-1}$	Source
2.82	6270	109258	8639	Neugebauer et al. [34]
		105313	5354	Avrami [36]
		140866	55600	Amado et al. [37]

condition, the specimen is considered to have yielded according to ASTM D7791−17.

Wöhler SN curves are constructed, and the experimental data are fitted using a Basquin relationship, as described in Eq. (2):

$$\sigma_a = \frac{C_1}{N_f^{C_2}} \tag{2}$$

where σ_a is the stress amplitude, N_f the number of cycles to failure and C_1 and C_2 are fitting coefficients. The scatter of the fatigue data is assessed by computing the estimated regression variance, assumed to be uniform for the whole fatigue life range, expressed in Eq. (3).

$$S^2 = \frac{\sum_{i=1}^{n} \left(\sigma_{a,i} - \widehat{\sigma}_{a,i}\right)^2}{n-p} \tag{3}$$

where $\sigma_{a,i}$ is the i-th fatigue amplitude data point, $\widehat{\sigma}_{a,i}$ is its estimator, n is the number of data elements, and p is the number of parameters in the regression (p = 2).

Additional fatigue tests are carried out on both MJF and HP specimens to evaluate the influence of temperature during fatigue testing. To this end, an infrared thermal imaging camera (IRtech Fotric 348A, E Instrument Group s.r.l., Italy) is positioned at a fixed distance of 30 cm from the specimen during the test and the collected images are analyzed leveraging the AnalyzIR software (Version 5.0.7.117, E Instrument Group s.r.l., Italy) to extract punctual temperature values along the specimens' longitudinal axis. The camera has an uncertainty of ± 2 °C in the measured temperature interval, with an acquisition frequency set at 16 fps and an emissivity parameter of 0.9. Two loading conditions are selected: a high-stress case, representative of low-cycle fatigue, and a low-stress case, representative of high-cycle fatigue.

2.4. HP process optimization

Once the role of crystallinity in fatigue properties is established, a process-oriented optimization strategy can be defined. The objective is to minimize the processing time while achieving a target degree of crystallinity.

A reduced cooling rate is known to increase the crystallinity of PA12; however, applying slow cooling over the entire temperature range is inefficient. Therefore, the process is optimized by limiting the reduced cooling rate to the effective crystallization window.

The crystallization kinetics under non-isothermal conditions are described using the Nakamura model [32–34], expressed in its integral form as per Equation (4):

$$\frac{\chi_c(T)}{\chi_{c,max}} = \alpha(t) = 1 - e^{-\left(\int_0^t K(T)d\tau\right)^n} \tag{4}$$

where $\alpha(t)$ is the relative crystallinity, n is the Avrami exponent, and $K(T)$ is the temperature-dependent crystallization rate. The kinetic parameter $K(T)$ is defined in Equation (5):

$$K(T) = \log(2)^{\frac{1}{n}} \left(\frac{1}{t_{\frac{1}{2}}}\right) \tag{5}$$

with the half-crystallization time $t_{1/2}$ expressed in Equation (6):

$$\frac{1}{t_{\frac{1}{2}}} = K_0 e^{-\frac{U}{R(T-T_\infty)}} e^{-\frac{K_G(T+T_m)}{2T^2\Delta T}} \tag{6}$$

where $T_\infty = T_g - 30\ K$ and $\Delta T = T_m - T$.

Since a complete kinetic characterization of HP 3D reusability PA12 is not available, kinetic parameters from literature for PA12 (EOS PA2200) are adopted. To account for variability, multiple parameter sets are considered (Table 2), representing different crystallization kinetics reported in literature [34–37].

The model is numerically integrated over the imposed thermal history to predict the evolution of crystallinity. The optimal cooling strategy is defined as the minimum time required to reach 99% of the maximum crystallinity ($\alpha = 0.99$) within the crystallization temperature range.

To validate the proposed approach, DSC measurements are performed on specimens processed under optimized cooling conditions, and the predicted crystallinity is compared with experimental values. Specifically, three validation tests are run: (i) Test 1 should reach the maximum crystallinity if the material follows the parameters reported by Neugebauer et al. [34], (ii) Test 2 should reach the maximum crystallinity according to the parameters reported by Amado et al. [37], and (iii) Test 3 produces a full cooling ramp at 0.5 °C/min from 170 °C to room temperature to obtain the full crystallization exotherm at the set cooling rate.

For these tests, neat powder specimens of approx. 5 mg were heated at 20 °C/min until 200 °C, kept at 200 °C for 2 min, cooled down at

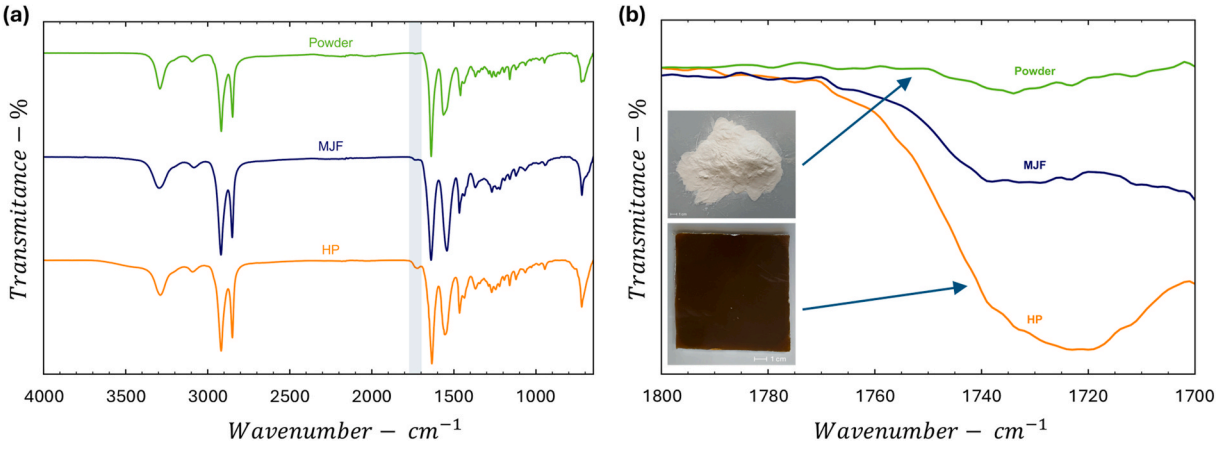

Fig. 4. FT-IR normalized and baseline corrected spectra of the PA12 powder, HP and MJF samples: (a) in the range 4000-650 cm−1 (spectra have been vertically shifted to improve clarity) and (b) in the range 1800-1700 cm−1.

Table 3
Main FT-IR absorption bands (cm^{-1}) and their measurements for PA12 powder, MJF and HP samples.

Vibration Type – cm^{-1}	Powder	MJF	HP
$N-H$ stretching	3291	3293	3288
CH_2 asymmetric stretching	2917	2919	2918
CH_2 symmetric stretching	2848	2850	2849
$C=O$ stretching (Amide I)	1638	1639	1634
$C-N$ stretch/N–H bend (Amide II)	1563	1542	1554
CH_2 scissoring	1460	1466	1465
CH_2 twisting	1369	1369	1368
$C-N$ stretch/$C=O$ bending (Amide III)	1268	1268	1269
Skeletal motion ($CONH$)	1159	1159	1160
$C-C$ stretching	1122	1121	1121
$CONH$ in-plane bending	949	945	946
CH_2 rock	722	720	721

20 °C/min until 170 °C, and then slowly cooled at 0.5 °C/min for 1233 s, i.e., until the target temperature of 159.73 °C (Test 1), or for 1552 s, i.e., until the target temperature of 157.07 °C (Test 2), and then quickly cooled down in liquid nitrogen. The resulting crystallinity was then measured with a heating ramp at 10 °C/min, as in the case of the MJF and HP specimens.

3. Results and discussion

This section initially focuses on the characterization of the base powder, the MJF and the HP specimens under a preliminary molecular, thermal and CT-based metrological analysis. The results are then leveraged to describe the effect of manufacturing induced characteristics on fatigue resistance.

3.1. Thermo-physical and metrological characterization

Fig. 4(a) reports the normalized and baseline corrected spectra of the PA12 powder, HP and MJF samples. Table 3 reports the corresponding infrared spectra peaks, which are in good agreement with literature [21,27]. Large coherence is found among the three analyzed spectra, showing a limited influence of the manufacturing technologies on the material composition.

A specific discrepancy is highlighted in Fig. 4(a) and magnified in Fig. 4(b), where the FT-IR spectra provide clear evidence of thermo-oxidative degradation in PA12. Degradation in polyamides is typically manifested by increased absorbance in the carbonyl region (1750–1700 cm^{-1}) [27,38–40]. Eriksson et al. [41] reported that the growth of these bands may result from differences in hydrogen bonding, the formation of additional carbonyl groups, changes in their conformation, and temperature-dependent effects. This process produces also a visible color change from the white virgin powder to the yellow/brown tone observed in HP specimens - Fig. 4(b). A continuous exposition of the polyamide to heating and cooling cycles during the MJF process and the subsequent hot pressing, incrementally increases this effect, producing increasing thermo-oxidative degradation and a color shift.

Fig. 5 depicts the thermograms of PA12 powder, MJF and HP specimens, including the first heating, cooling, and second heating scans. In the first heating scan, only one endothermic melting peak was observed at 181-188 °C, indicating that the PA12 in all the examined forms was predominantly in the γ crystalline phase [42].

Table 4 collects the parameters obtained thanks to the DSC analysis. The characteristics of PA12 powder are consistent with literature data, which report T_g in the range of 40–50 °C and T_m between 170 and 180 °C [43,44]; values of χ_c, T_g, T_m obtained for the MJF specimens are also in good agreement with previous studies [20,21].

There is a clear impact of the manufacturing process on the properties of the PA12: the ratio between amorphous and crystalline phases is shifted by the specimens' thermal history. Slower cooling rates, as in MJF and HP slow cooling specimens yielded a higher crystallinity with respect to HP manufactured with standard procedure. This factor is also visible in ΔH_m, while there is no effect given by the manufacturing process on T_g and T_m.

Results collected in Table 4 focus on the first heating profile of the DSC analysis; all the specimens underwent cooling and subsequently a second heating profile. Results obtained in these later stages are coherent with literature [28] and among the different specimens, demonstrating a negligible material sensitivity to the manufacturing process after remelting. More specifically, in the second heating scan, all samples show the same melting temperature, of approx. 179-180 °C, which suggests that the degradation and oxidation resulting from FTIR tests is only marginal and does not lead to considerable decrease in molecular weight.

The thermograms of PA12 powder in N_2 and in air are depicted in Fig. 6.

A very limited mass loss (∼ 0.6%) is recorded in air before 220 °C, which corresponds to the temperature used during hot pressing to consolidate the plates. The samples are not dried prior to testing (at 100 °C the mass loss is ≈ 0.2%) and this initial weight reduction can be attributed to the release of moisture. The decision not to dry the powder

Table 4
Main results of the DSC analysis (first heating scan) for the different manufacturing techniques.

Specimen	T_g - °C	T_m - °C	$\Delta H_m - J/g$	χ_c - %
Powder	50.1	188.6	117.9	56.4
MJF	38.6	181.9	66.1	31.6
HP	37.8	181.5	46	22.0
HP slow cooling	37.0	181.3	64.1	30.7

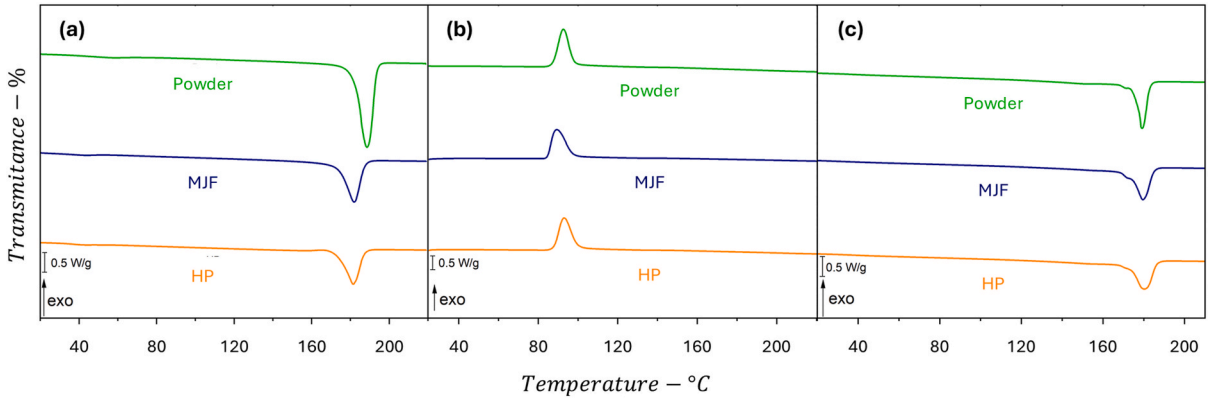

Fig. 5. DSC thermograms of PA12 powder, standard HP and MJF sample: a) first heating scan; b) cooling scan; c) second heating scan.

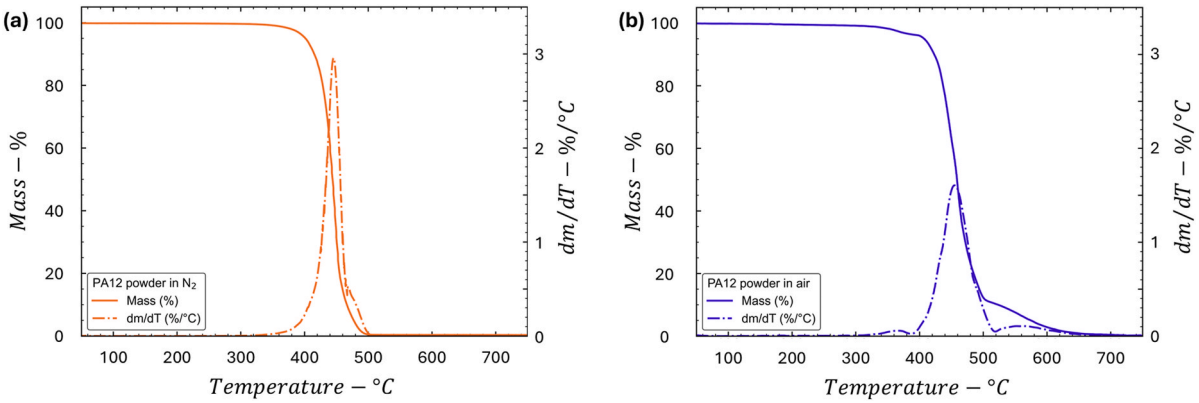

Fig. 6. Thermograms of PA12 powder showing residual mass and its derivative in N_2 (a) and in air (b).

is intentional, to better reproduce industrially relevant conditions, where the residual humidity of PA12 is generally considered negligible due to its low water uptake [45,46]. No residual mass was detected after 750 °C in air, suggesting that possible contaminants in the powder are either present in negligible amounts or completely decomposed below this temperature.

Fig. 7 shows the storage modulus, the loss modulus and the loss factor trends for the HP and MJF specimens.

The storage modulus, correlated to material stiffness, is higher for HP samples at temperatures below T_g, whereas above T_g the opposite trend is observed. Thus, by increasing the temperature, the HP specimens became softer than their MJF counterpart. By analyzing the loss modulus, which represent the viscous contribution of the polymer, and the tan(δ), representing the fraction of energy dissipated as heat, it is evident that the HP specimens exhibit a larger viscous contribution and an increasing energy dissipation than their MJF counterparts. The T_g of the two samples, measured at the *tan* δ maximum, is similar (56.8 °C for MJF and 59.6 °C for HP), in good agreement with data from DSC.

Computed tomography three-dimensional geometrical reconstruction for a standard HP specimen is presented in Fig. 8(a). The analysis reveals that the HP specimen shows negligible internal porosity. An in-depth description of the MJF porosity is presented in Ref. [22], and a direct comparison between HP and MJF shows the superior yield of the traditional manufacturing technologies with respect to MJF: during hot pressing high pressure is applied to the melted polymer, which leads to a closing action of the pores. On the other and, during MJF pores can be generated due to usage of sub-optimal printing parameters, resulting in lack of fusion and intralayer porosity [47]. These manufacturing induced defects are well known in literature [48,49], and – as presented in Fig. 8(b) – are mainly located in the center of the specimen geometry. This is a manufacturing induced feature: a detailing agent is deposited on the powder at the geometry contours to yield a higher degree of fidelity in MJF components.

3.2. Mechanical characterization

As depicted in Fig. 9, the quasi-static behavior of the PA12 produced via HP is typical for a polyamide. The elastic modulus is measured at 1.6 GPa and σ_y is found at $\sim$ 44 MPa. A complete analysis of the quasi-static properties and a comparison with MJF ones is provided in Table 5. Standard HP specimens' stress-strain curve shows an initial linear relation followed by a sudden yield and a long plastic plateau before the final failure. Focusing on the elastic modulus, the reported values are highly consistent with the storage modulus results obtained via DMTA; moreover, these results align well with previous findings on MJF [4,15,21,50]. It is worth noting that PA12 produced via HP expresses similar properties in terms of elastic modulus and yield stress if compared to the same material produced with the MJF technique, however, the additive manufacturing process significantly reduces the strain at failure, ε_B, measured around 10-12% [15,22].

Different sets of MJF and HP specimens are tested under fatigue loading at two different operating frequencies 3Hz and 5Hz. The results are presented in Fig. 10, where in 10(a) are collected the Wöhler curves of the HP specimens, and in 10(b) the Wöhler curves of the MJF specimens. Experimental data are fitted, and the resulting coefficients are presented in Table 6.

Clear trends are visible in the data: fatigue resistance is deeply impacted by both manufacturing process and testing frequency.

Comparing Fig. 10(a) and (b), it can be noted that at a given testing frequency, the fatigue resistance of MJF specimens outperforms the HP ones. Metrologically, this is a counter-intuitive result: as testified by the CT-based 3D geometrical reconstructions of the HP specimen, the obtained geometry is completely bulk, where only a limited number of pores is present. In contrast, MJF specimens are characterized by a significantly larger dispersion of pores, with different size and shapes [22], undoubtedly detrimental to the fatigue resistance of the specimens. Hence, the causes of the reduced performance of the HP specimens must be reconducted to the material properties induced by the manufacturing process. As reported in Table 4, the specimens obtained via HP are characterized by a lower crystallinity (22%) with respect to the MJF ones (31%). This discrepancy in the microstructure of the specimens is directly related to the cooling rates imposed during the manufacturing process and is impacting the fatigue resistance as it will be clarified in the following paragraphs.

Regardless of the manufacturing process, the specimens tested at 3Hz show higher fatigue resistance with respect to the ones tested at 5Hz. This effect is evident in the specimens realized with HP technology, where a drop of $\sim$ 30% is registered in the fatigue resistance. MJF specimens are instead less prone to a reduction of the fatigue properties when the testing frequency is increased. Experimental data show several overlapping between the two curves, and this is especially true for low cycle fatigue (LCF) conditions (high loads imposed).

The impact of the testing frequency on the fatigue properties is a well-known effect in the fatigue of polymeric materials. As reported in literature [11], the application of cyclic loads to the polymeric matrix activates viscoelastic phenomena, dissipating the mechanical energy into heat. This is a severe effect, since material properties sensibly decay with the increment of the temperature and the consequences of thermal fatigue dominate over the other sources of failure. This is particularly true for polymers with a low to medium degree of crystallinity and a glass transition temperature only slightly higher than room temperature, such as PA12.

These two observations can be combined considering thermal fatigue: the HP specimens, characterized by a lower crystallinity with respect to the MJF ones – as testified by higher tan(δ) measured in the DMTA analysis – are more prone to viscous phenomena, generating

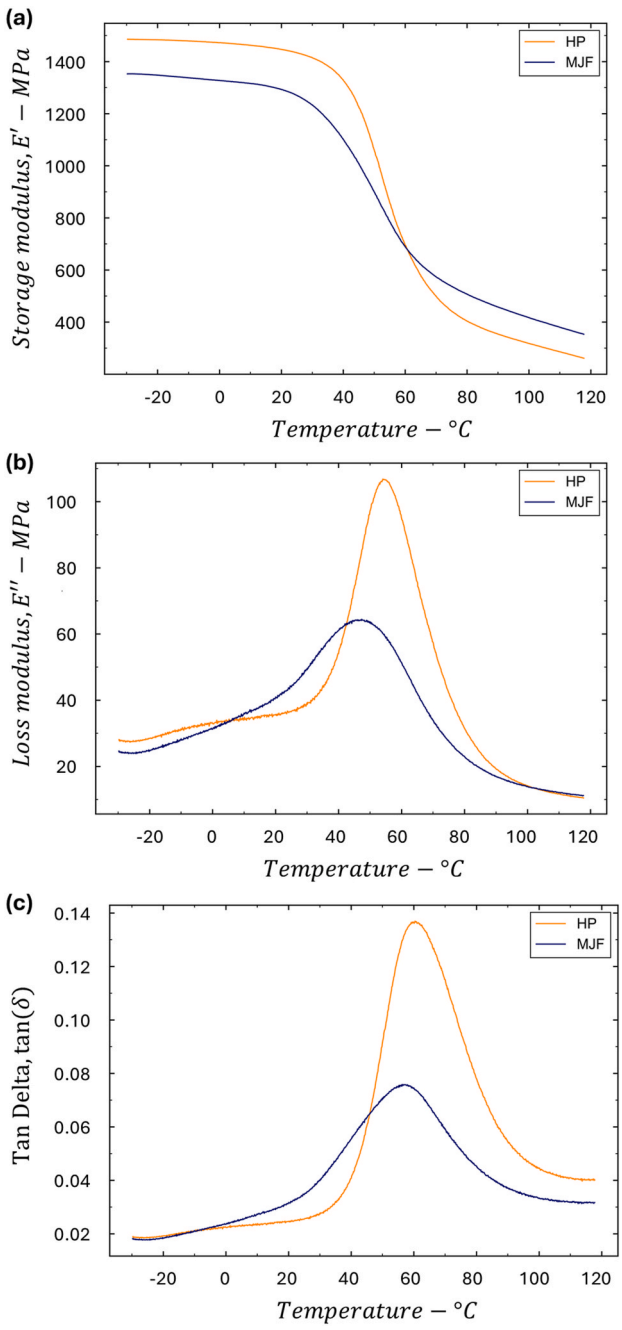

Fig. 7. DMA results of standard HP and MJF specimens: (a) storage modulus, (b) loss modulus, and (c) tan delta.

more heat and thus showing a reduced fatigue resistance if compared to MJF. This effect is more pronounced when the testing frequency is increased, causing an increment of the heat generation.

It should be noted that the present characterization relies solely on the overall degree of crystallinity obtained via DSC and does not capture morphological features such as spherulite size or crystal perfection, which can also influence fatigue resistance independently of crystallinity. For instance, Salazar et al. [24] reported that, for PA12 processed via injection molding and SLS, fracture-related fatigue parameters decreased with increasing spherulite size despite a higher overall crystallinity in the injection-molded samples. Since the cooling rate governs both nucleation and growth kinetics, it is reasonable to expect that it influenced crystal morphology in addition to crystallinity in the specimens of this study; a dedicated morphological investigation (e.g., via polarized optical microscopy or X-ray diffraction) is identified as a relevant direction for future work.

To further prove this effect, thermographic tests are conducted on MJF and HP specimens tested at 5 Hz. Fig. 11 compares the behavior of an HP and a MJF specimen tested in the high cycle fatigue (HCF) regime (low load imposed). Thermographic analyses show a coherent behavior between the two specimens: the surface temperature of the specimens gradually increases in the first 1000 cycles, where it reaches a plateau. In this condition, the heat generated by the viscous effects is balanced by the heat exchanged with the environment. A strong correlation is found between the evolution of the specimen temperature and the specimen stiffness: an increment in the specimen temperature is directly related to a decrement in stiffness, proving once again the detrimental effect of temperature on the mechanical properties.

A second test is conducted in the low cycle fatigue (LCF) regime, where the applied loads are higher – results are presented in Fig. 12. In this condition, the behaviors observed in the previous analysis are extremized: the temperature increment is sensible, driven by the higher energy input in the system, and the thermal equilibrium between the specimens and the environment is not reached before the specimen failure. The specimen manufactured with MJF technology may reach the equilibrium condition in the zone (III) (Fig. 12 (a)) but shortly before the complete failure.

A beneficial effect on the fatigue life of the HP specimens is provided by the manufacturing process characterized by extended cooling. Fig. 13 compares the curves obtained at the same testing frequency (5 Hz) for MJF, HP and HP with extended cooling ("EC"). The fatigue curve for HP specimens with extended cooling displays a clear improvement with respect to the standard one and has comparable in LCF and improved in HCF results when compared to the MJF curve. This improvement is directly related to the change in the microstructure: higher crystallinity is linked to lower sensitivity to self-heating and therefore less impact of the thermal effects. The comparison with MJF shows instead the effect of manufacturing induced defects: even though the LCF region is still dominated by thermal effects, the HCF region shows an improvement of the HP specimens with extended cooling with respect to MJF ones. The specimens' failure mechanism is, at these loads, dominated by the crack nucleation and the crack growth. MJF specimens characterized by a sensible larger defect population with respect to HP ones, are more prone to fail.

Given the limited cooling rates imposed in the manufacturing process, the influence of residual stresses is considered marginal in the presented fatigue analysis.

3.3. HP process optimization

Once the crucial impact of crystallinity on fatigue properties is understood, a process parameter optimization can be performed. Fig. 14(a) shows the range of crystallization kinetics obtained from the literature parameters reported in Table 2. The variability in K_G and K_0 is directly reflected in the predicted crystallization rates, resulting in a bounded kinetic domain. The two limiting cases, corresponding to the fastest (Test 1) and slowest kinetics (Test 2) - Neugebauer et al. [34] and Amado et al. [37] respectively - were selected for experimental validation.

The time required to reach 99% of the maximum crystallinity ($\alpha = 0.99$) was predicted as $t = 1233$ s at $T = 159.7°C$ for Neugebauer parameters and $t = 1552$ s at $T = 157.0°C$ for Amado parameters. These conditions were reproduced experimentally using DSC, yielding relative crystallinity values of $\alpha = 0.82$ and $\alpha = 1$, respectively. These values are calculated considering the maximum crystallinity obtainable at 0.5 °C/min, viz. the one effectively obtained on the sample HP "EC", equal to 31.1%. The experimental results, reported in Fig. 14(a), show good agreement with model predictions and confirm the capability of the adopted kinetic framework to capture the crystallization behavior of PA12 within the investigated range. Additional experimental evidence is provided by Test 3, where the experimental peak was integrated to

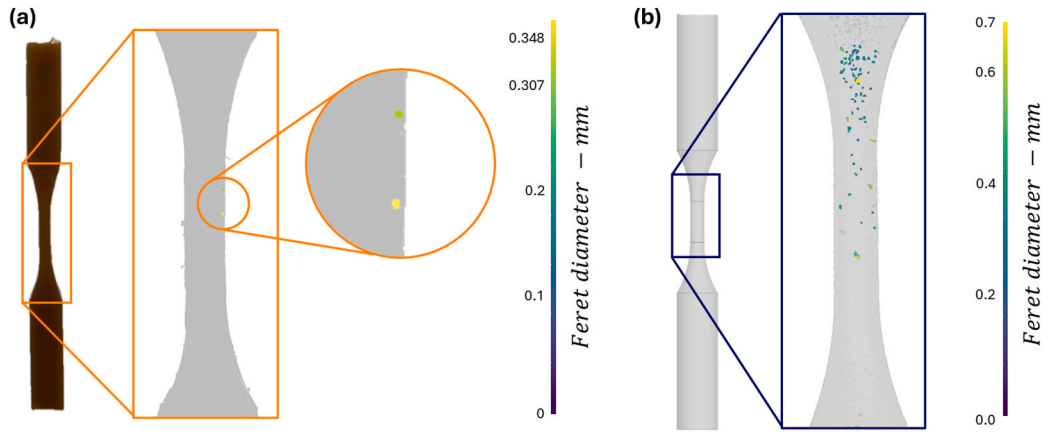

Fig. 8. 3D CT-based geometrical reconstruction of a standard HP specimen (a) and MJF specimen (b). The pores' dimension is indicated with Feret diameter. Image (b) is adapted from Ref. [22].

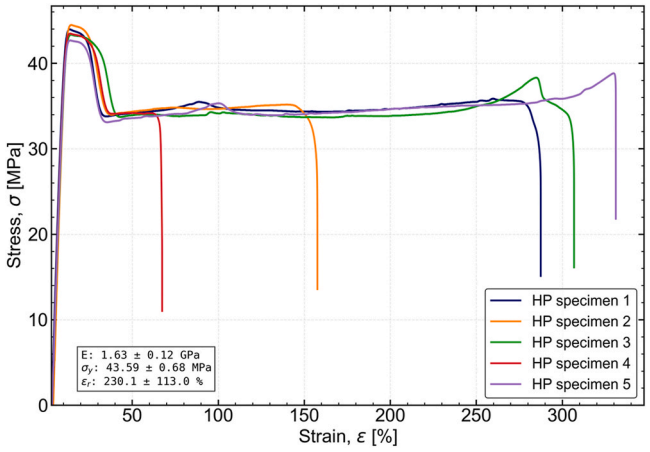

Fig. 9. Quasi-static response of the HP tensile specimens.

Table 5
Comparison of quasi-static properties for HP and MJF PA12. Properties for MJF are retrieved from Ref. [15]. The elastic modulus reported in literature shows significant variability reflecting the influence of process parameters, build orientation, and testing methodologies. The average value reported here was computed after excluding clear outliers to ensure a representative estimate. Due to the absence of a distinct yield point in MJF PA12, yielding is defined as the deviation from linear elastic behavior.

Specimen	E - *GPa*	σ_y - *MPa*	ε_y – %	σ_B - *MPa*	ε_B – %
HP	1.6 ± 0.12	43.6 ± 0.7	12 ± 3	36.5 ± 0.7	230 ± 113
MJF	1.4 ± 0.2	22 ± 5	1.5 ± 0.5	45.4 ± 4.9	10 ± 3.4

produce an experimental crystallinity vs. time sigmoid. This crystallization kinetic fits well the limiting conditions expressed by Nakamura model.

Notably, the slowest kinetic provides a conservative estimate of the crystallization process, safely bounding the experimental response. Based on this observation, the slowest kinetic is adopted as a reference for process design. Fig. 14(b) presents the optimized cooling profile derived from the model. The process is structured in four stages. After melting, a rapid cooling stage (1) reduces the temperature to $T = 170°C$ at 20 °C/min, minimizing non-effective processing time. An isothermal hold (2) of 120 s is then applied to promote the onset of crystallization. Subsequently, a controlled slow cooling stage (3) at 0.5 °C/min is imposed for $t = 1552$ s, corresponding to the time required to reach near-complete crystallization according to the conservative kinetic model. Finally, a rapid cooling stage (4) brings the material to room temperature.

This approach defines a process window in which the cooling rate is selectively reduced only within the effective crystallization range, enabling the maximization of crystallinity while minimizing the overall processing time. The proposed methodology can be extended to complex geometries by locally adapting the thermal history to match the target cooling profile in regions critical for fatigue performance. It should be noted that the kinetic parameters are taken from literature and not directly identified for the specific powder used in this study. Therefore, the proposed results are intended to provide a possible methodology rather than a complete characterization of the material.

4. Conclusions

This work investigated the role of process-controlled crystallinity in governing the fatigue response of PA12 produced by Multi Jet Fusion and hot pressing. MJF and HP specimens were manufactured from the same PA12 powder batch, while different cooling strategies were applied during hot pressing to isolate the influence of thermal history on microstructure, viscoelastic dissipation and fatigue resistance.

The results demonstrate that the fatigue behavior of PA12 is strongly governed by the crystallinity induced by the manufacturing process. Standard HP specimens exhibited lower crystallinity than MJF specimens. Despite their negligible internal porosity – typically expected to enhance fatigue resistance – they showed inferior fatigue performance. This behavior is associated with higher viscoelastic dissipation and more pronounced self-heating under cyclic loading, as confirmed by DMTA and infrared thermography measurements. The reduced crystallinity increases the fraction of the amorphous phase, promoting molecular mobility and energy dissipation, which accelerates thermal softening and premature failure. Overall, these findings highlight that, under the investigated conditions, crystallinity and the resulting thermomechanical stability play a dominant role over porosity in controlling the fatigue response of PA12.

The influence of testing frequency further confirmed the relevance of thermal-fatigue coupling. Increasing the loading frequency promoted self-heating and reduced fatigue life, especially in the low-crystallinity HP specimens. In contrast, the more crystalline MJF specimens were less sensitive to frequency, indicating that a higher crystalline fraction reduces the mobility of the amorphous phase and limits heat generation during cyclic loading.

The extended cooling protocol applied to HP specimens proved effective in increasing crystallinity to values comparable with those of MJF specimens. As a result, HP specimens processed with extended cooling showed a marked improvement in fatigue resistance. Their

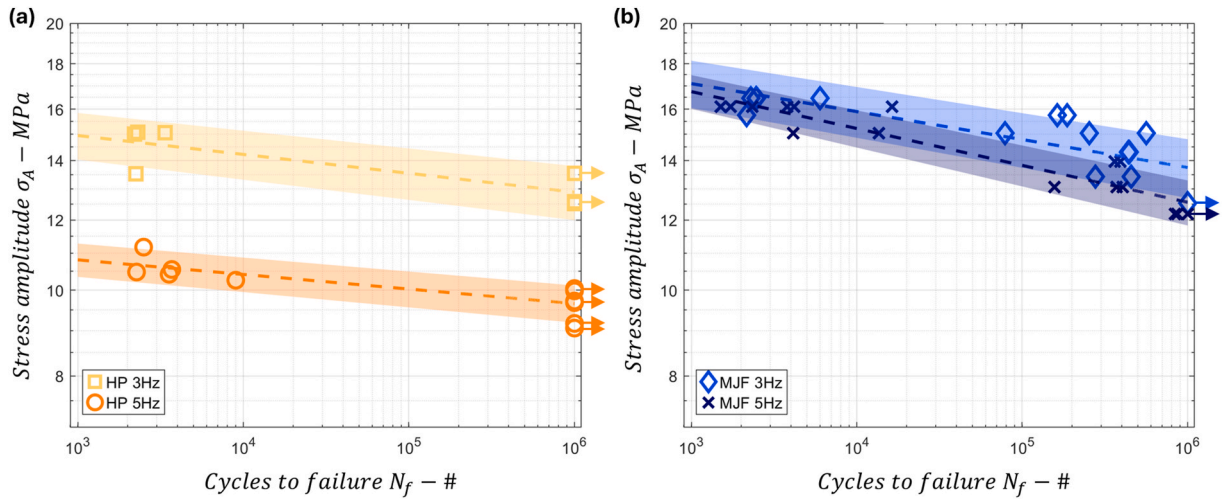

Fig. 10. Wöhler curves of HP (a) and MJF (b) specimens tested at R = 0.1 with different testing frequencies.

Table 6
Fitting parameters C_1, C_2, errors and testing details for MJF and HP specimens tested at R = 0.1. Hot pressed specimens characterized by the extended cooling process are labelled as "EC".

Geometry	C_1	C_2	$S^2 - MPa^2$	# spec.s	# run out spec.s
MJF 3Hz	21.2590	0.0315	0.6706	17	2
MJF 5Hz	22.3261	0.0416	0.3292	17	2
HP 3Hz	17.3101	0.0213	0.4986	7	3
HP 5Hz	12.1199	0.0165	0.1327	12	7
HP 5Hz "EC"	17.5272	0.0123	0.0635	6	2

behavior became comparable to that of MJF specimens in the low-cycle fatigue regime and superior in the high-cycle fatigue regime, where the lower defect population of HP specimens becomes beneficial.

Based on these findings, a cooling-profile optimization strategy was proposed using the Nakamura crystallization model. The optimized process selectively reduces the cooling rate within the effective crystallization window, allowing crystallinity to be maximized while limiting the overall processing time. Experimental validation confirmed that the adopted kinetic framework provides a useful basis for designing cooling profiles aimed at controlling PA12 crystallinity.

Overall, the results show that tailoring the cooling history is an effective process-level strategy to enhance the fatigue resistance of PA12. More broadly, the study demonstrates that manufacturing-induced crystallinity can be used as a design variable for improving

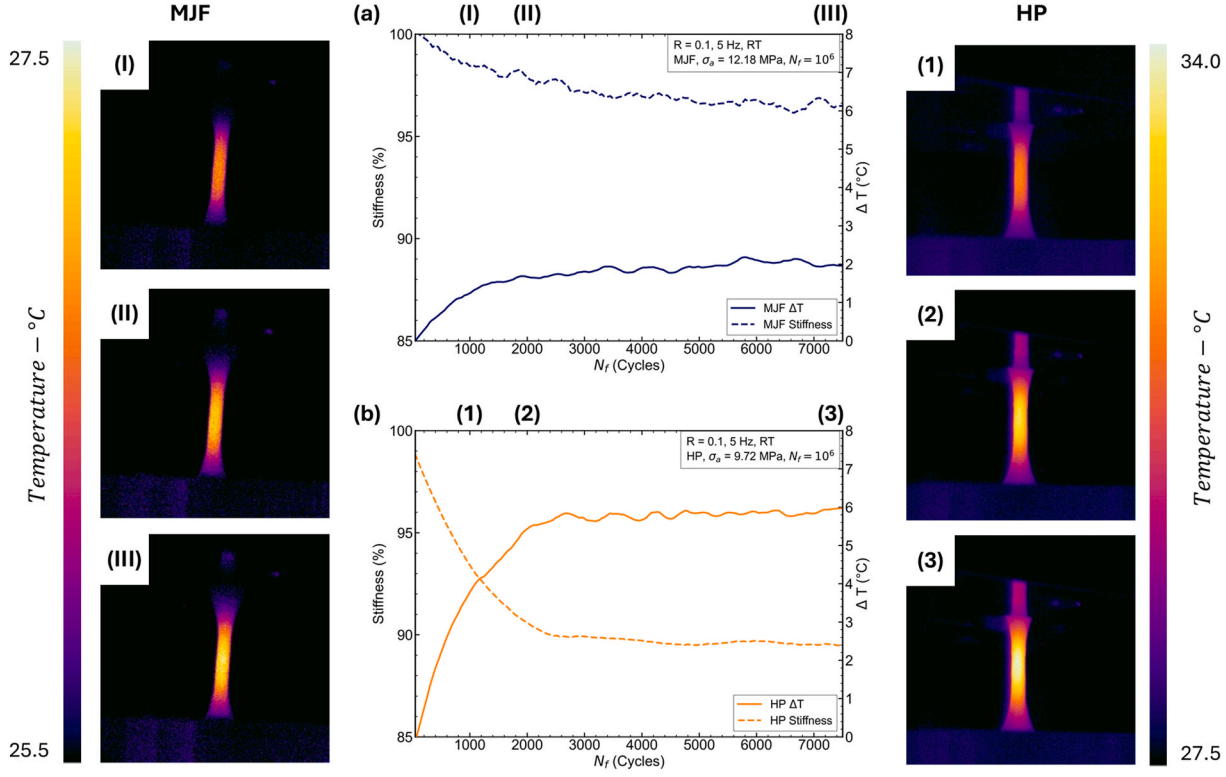

Fig. 11. Comparison of measured temperature and stiffness value during low stress fatigue testing (HCF) for MJF (a) and HP (b) specimens. The charts are correlated by IR thermograms showing the specimen's surface at different testing times.

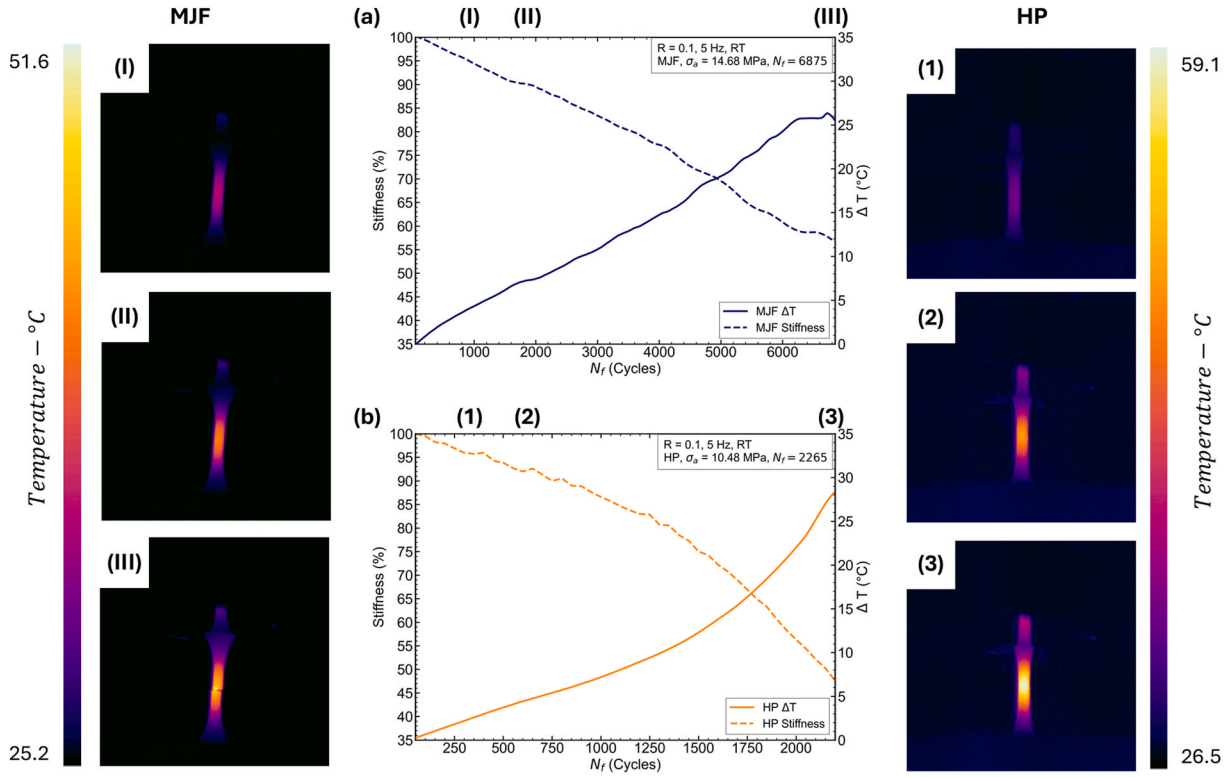

Fig. 12. Comparison of measured temperature and stiffness value during high stress fatigue testing (LCF) for MJF (a) and HP (b) specimens. The charts are correlated by IR thermograms showing the specimen's surface at different testing times.

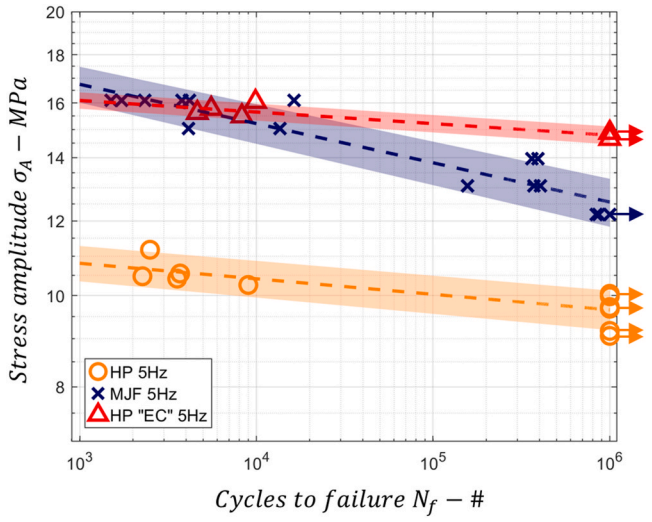

Fig. 13. Comparison of the Whöler curves of MJF, HP and HP with extended cooling tested at R = 0.1 at 5 Hz.

the durability of polymer components produced by powder-bed-based additive manufacturing and alternative consolidation routes. Future work should extend this approach to MJF-specific thermal management strategies and to more complex geometries, including lattice structures and components with spatially varying thermal histories.

CRediT authorship contribution statement

Raffaele De Biasi: Writing – original draft, Writing – review & editing, Visualization, Software, Methodology, Investigation, Formal analysis, Data curation, Conceptualization. **Damiano Foltran:** Writing – original draft, Visualization, Software, Investigation, Formal analysis, Data curation. **Giulia Fredi:** Writing – original draft, Writing – review & editing, Supervision, Methodology, Formal analysis, Investigation, Conceptualization. **Matteo Perini:** Writing – review & editing, Resources. **Filippo Berto:** Writing – review & editing, Supervision, Funding acquisition. **Matteo Benedetti:** Writing – review & editing, Supervision, Conceptualization.

Declaration of generative AI and AI-assisted technologies in the writing process

During the preparation of this work the authors used ChatGPT (based on GPT– 4o – OpenAI) to reorganize notes and improve the manuscript readability. After using this tool, the authors reviewed and edited the content as needed and took full responsibility for the content of the published article.

Funding sources

Funded by the European Union (ERC, 101093897 Butterfly). Views and opinions expressed are however those of the author(s) only and do not necessarily reflect those of the European Union or the European Research Council Executive Agency. Neither the European Union nor the granting authority can be held responsible for them.

Declaration of competing interest

The authors declare that they have no known competing financial interests or personal relationships that could have appeared to influence the work reported in this paper.

Data availability

Data will be made available on request.

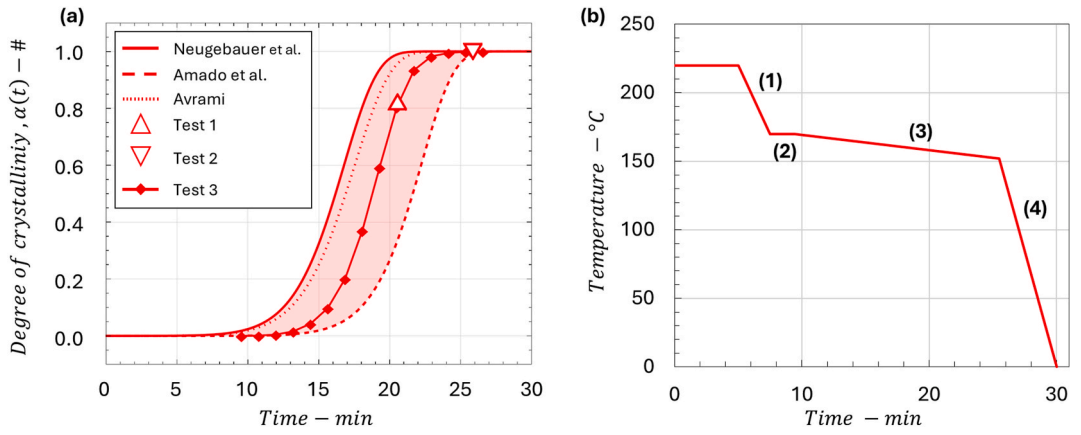

Fig. 14. (a) Comparison of PA12 crystallization kinetics calculated with the Nakamura model, following different material characterizations available in literature and experimental validations. (b) Optimized cooling profile to obtain maximum crystallinity in minimum time.

References

[1] Yang F, Zobeiry N, Mamidala R, Chen X. A review of aging, degradation, and reusability of PA12 powders in selective laser sintering additive manufacturing. Mater Today Commun 2023;34:105279. https://doi.org/10.1016/j.mtcomm.2022.105279.

[2] Zakręcki A, Cieślik J, Bazan A, Turek P. Innovative approaches to 3D printing of PA12 forearm orthoses: a comprehensive analysis of mechanical properties and production efficiency. Materials 2024;17:663. https://doi.org/10.3390/ma17030663.

[3] Jafferson JM, Chatterjee D. A review on polymeric materials in additive manufacturing. Mater Today Proc 2021;46:1349–65. https://doi.org/10.1016/j.matpr.2021.02.485.

[4] Bahrami M, Abenojar J, Martínez MA. Comparative characterization of hot-pressed polyamide 11 and 12: mechanical, thermal and durability properties. Polymers 2021;13:3553. https://doi.org/10.3390/polym13203553.

[5] Sanders B, North M, Cant E, Jenkins M. Investigating secondary crystallisation of polyamide-12 using fast scanning calorimetry. Thermochim Acta 2025;745:179948. https://doi.org/10.1016/j.tca.2025.179948.

[6] Elsheikh A, Elmosalamy MA, Ma N, Eldeeb I, Showaib E, Ebied S. Enhancing joint efficiency in friction stir welding of PA66 using an induction-heated threaded pin and glass fiber reinforcement. J Mater Res Technol 2025;37:4153–64. https://doi.org/10.1016/j.jmrt.2025.06.193.

[7] Shen F, Yuan S, Chua CK, Zhou K. Development of process efficiency maps for selective laser sintering of polymeric composite powders: modeling and experimental testing. J Mater Process Technol 2018;254:52–9. https://doi.org/10.1016/j.jmatprotec.2017.11.027.

[8] Bai J, Song J, Wei J. Tribological and mechanical properties of MoS2 enhanced polyamide 12 for selective laser sintering. J Mater Process Technol 2019;264:382–8. https://doi.org/10.1016/j.jmatprotec.2018.09.026.

[9] Sillani F, Kleijnen RG, Vetterli M, Schmid M, Wegener K. Selective laser sintering and multi jet fusion: process-induced modification of the raw materials and analyses of parts performance. Addit Manuf 2019;27:32–41. https://doi.org/10.1016/j.addma.2019.02.004.

[10] Speranza V, Salomone R, Pantani R. Effects of pressure and cooling rates on crystallization behavior and morphology of isotactic polypropylene. Crystals 2023;13:922. https://doi.org/10.3390/cryst13060922.

[11] Sauer JA, Richardson GC. Fatigue of polymers. Int J Fract 1980;16:499–532. https://doi.org/10.1007/BF02265215.

[12] Crawford RJ, Benham PP. Cyclic stress fatigue and thermal softening failure of a thermoplastic. J Mater Sci 1974;9:18–28. https://doi.org/10.1007/BF00554752.

[13] Van Hooreweder B, Kruth J-P. High cycle fatigue properties of selective laser sintered parts in polyamide 12. CIRP Ann 2014;63:241–4. https://doi.org/10.1016/j.cirp.2014.03.060.

[14] Jyotishkumar P, Jenny J, Senthilkumar K, Aswathy J, Nishar H. Polymer crystallization: methods, characterization, and applications. First. WILEY-VCHGmbH; 2023.

[15] Avanzini A, Battini D, Pandini S. Static and fatigue behavior in presence of notches for polyamide 12 (PA12) additively manufactured via multi jet Fusion™ process. Int J Fatig 2022;161:106912. https://doi.org/10.1016/j.ijfatigue.2022.106912.

[16] Ma N, Liu W, Ma L, He S, Liu H, Zhang Z, et al. Crystal transition and thermal behavior of nylon 12. E-Polymers 2020;20:346–52. https://doi.org/10.1515/epoly-2020-0039.

[17] Zhao M, Wudy K, Drummer D. Crystallization kinetics of polyamide 12 during selective laser sintering. Polymers 2018;10:168. https://doi.org/10.3390/polym10020168.

[18] Teo HWB, Chen K, Tran VT, Du H, Zeng J, Zhou K. Non-isothermal crystallization behaviour of polyamide 12 analogous to multi-jet fusion additive manufacturing process. Polymer (Guildf) 2021;235:124256. https://doi.org/10.1016/j.polymer.2021.124256.

[19] Chen K, Koh ZH, Le KQ, Teo HWB, Zheng H, Zeng J, et al. Effects of build positions on the thermal history, crystallization, and mechanical properties of polyamide 12 parts printed by multi jet fusion. Virtual Phys Prototyp 2022;17:631–48. https://doi.org/10.1080/17452759.2022.2046478.

[20] Rosso S, Meneghello R, Biasetto L, Grigolato L, Concheri G, Savio G. In-depth comparison of polyamide 12 parts manufactured by multi jet fusion and selective laser sintering. Addit Manuf 2020;36:101713. https://doi.org/10.1016/j.addma.2020.101713.

[21] Cai C, Tey WS, Chen J, Zhu W, Liu X, Liu T, et al. Comparative study on 3D printing of polyamide 12 by selective laser sintering and multi jet fusion. J Mater Process Technol 2021;288:116882. https://doi.org/10.1016/j.jmatprotec.2020.116882.

[22] De Biasi R, Romanelli L, Santus C, Perini M, Berto F, Benedetti M. Fatigue life prediction of multi jet fusion-manufactured polyamide12 lattice structures using the average strain energy density method. Int J Fatig 2026;206:109452. https://doi.org/10.1016/j.ijfatigue.2025.109452.

[23] Van Hooreweder B, Moens D, Boonen R, Kruth J-P, Sas P. On the difference in material structure and fatigue properties of nylon specimens produced by injection molding and selective laser sintering. Polym Test 2013;32:972–81. https://doi.org/10.1016/j.polymertesting.2013.04.014.

[24] Salazar A, Cano AJ, Rodríguez J. Mechanical and fatigue behaviour of polyamide 12 processed via injection moulding and selective laser sintering. Analysis based on Kitagawa-Takahashi diagrams. Eng Fract Mech 2022;275:108825. https://doi.org/10.1016/j.engfracmech.2022.108825.

[25] Simaafrookhteh S, Van Thillo T, Lomov SV, Ivens J. Crystallinity of neat and carbon fiber-reinforced polyamide-6 processed at different cooling rates. Compos Part A Appl Sci Manuf 2025;188:108520. https://doi.org/10.1016/j.compositesa.2024.108520.

[26] Beretta S. More than 25 years of extreme value statistics for defects: fundamentals, historical developments, recent applications. Int J Fatig 2021;151:106407. https://doi.org/10.1016/j.ijfatigue.2021.106407.

[27] Zhang J, Adams A. Understanding thermal aging of non-stabilized and stabilized polyamide 12 using 1H solid-state NMR. Polym Degrad Stab 2016;134:169–78. https://doi.org/10.1016/j.polymdegradstab.2016.10.006.

[28] Cobian L, Maire E, Adrien J, Freitas U, Fernández-Blázquez JP, Monclús MA, et al. Effect of sample dimensions on the stiffness of PA12 lattice materials fabricated using powder bed fusion. Addit Manuf 2024;93:104382. https://doi.org/10.1016/j.addma.2024.104382.

[29] Pavan M, Faes M, Strobbe D, Van Hooreweder B, Craeghs T, Moens D, et al. On the influence of inter-layer time and energy density on selected critical-to-quality properties of PA12 parts produced via laser sintering. Polym Test 2017;61:386–95. https://doi.org/10.1016/j.polymertesting.2017.05.027.

[30] Safai L, Cuellar JS, Smit G, Zadpoor AA. A review of the fatigue behavior of 3D printed polymers. Addit Manuf 2019;28:87–97. https://doi.org/10.1016/j.addma.2019.03.023.

[31] Reindl T, Meisner D, Hierl S. Benchmarking of plastic-based additive manufacturing processes. RTe Journal 2023:1–20. https://doi.org/10.58134/fh-aachen-rte_2023_002.

[32] Nakamura K, Watanabe T, Katayama K, Amano T. Some aspects of nonisothermal crystallization of polymers. I. Relationship between crystallization temperature, crystallinity, and cooling conditions. J Appl Polym Sci 1972;16:1077–91. https://doi.org/10.1002/app.1972.070160503.

[33] Nakamura K, Katayama K, Amano T. Some aspects of nonisothermal crystallization of polymers. II. Consideration of the isokinetic condition. J Appl Polym Sci 1973;17:1031–41. https://doi.org/10.1002/app.1973.070170404.

[34] Neugebauer F, Ploshikhin V, Ambrosy J, Witt G. Isothermal and non-isothermal crystallization kinetics of polyamide 12 used in laser sintering. J Therm Anal Calorim 2016;124:925–33. https://doi.org/10.1007/s10973-015-5214-8.

[35] Hosseini SMA, Schäkel M, Baran I, Janssen H, van Drongelen M, Akkerman R. Non-uniform crystallinity and temperature distribution during adjacent laser-assisted tape winding process of carbon/PA12 pipes. Int J Adv Manuf Technol 2020;111:3063–82. https://doi.org/10.1007/s00170-020-06215-8.

[36] Avrami M. Kinetics of phase change. I general theory. J Chem Phys 1939;7:1103–12. https://doi.org/10.1063/1.1750380.
[37] Amado A, Schmid M, Levy G, Wegener K. Characterization and modeling of non-isothermal crystallization of polyamide 12 and co-Polypropylene during the SLS process. In: 5th International polymers & moulds innovations conference; 2012. Ghent.
[38] Riedelbauch J, Rietzel D, Witt G. Analysis of material aging and the influence on the mechanical properties of polyamide 12 in the multi jet fusion process. Addit Manuf 2019;27:259–66. https://doi.org/10.1016/j.addma.2019.03.002.
[39] Pandelidi C, Blakis R, Lee KPM, Bateman S, Brandt M, Kajtaz M. Thermal and oxidative aging effects of Polyamide-11 powder used in multi-jet fusion. Polymers 2023;15:2395. https://doi.org/10.3390/polym15102395.
[40] Sanders B, Cant E, Amel H, Jenkins M. The effect of physical aging and degradation on the Re-Use of polyamide 12 in powder bed fusion. Polymers 2022;14:2682. https://doi.org/10.3390/polym14132682.
[41] Eriksson P-A, Boydell P, Eriksson K, M nson J-AE, Albertsson A-C. Effect of thermal-oxidative aging on mechanical, chemical, and thermal properties of recycled polyamide 66. J Appl Polym Sci 1997;65:1619–30. https://doi.org/10.1002/(SICI)1097-4628(19970822)65:8<1619::AID-APP18>3.0.CO;2-Q.
[42] Gogolewski S, Czerntawska K, Gastorek M. Effect of annealing on thermal properties and crystalline structure of polyamides. Nylon 12 (polylaurolactam). Colloid Polym Sci 1980;258:1130–6. https://doi.org/10.1007/BF01382456.
[43] NETZSCH Analyzing e Testing. Pa12 (Polyamide 12) engineering thermoplastics. https://analyzing-testing.netzsch.com/de/polymers-netzsch-com/engineering-thermoplastics/pa12-polyamide-12. [Accessed 9 September 2025].
[44] O' Connor HJ, Dowling DP. Comparison between the properties of polyamide 12 and glass bead filled polyamide 12 using the multi jet fusion printing process. Addit Manuf 2020;31:100961. https://doi.org/10.1016/j.addma.2019.100961.
[45] Seltzer R, de la Escalera FM, Segurado J. Effect of water conditioning on the fracture behavior of PA12 composites processed by selective laser sintering. Mater Sci Eng, A 2011;528:6927–33. https://doi.org/10.1016/j.msea.2011.05.045.
[46] Villani V, Ponticelli GS, Venettacci S, Guarino S. Effect of water absorption on the properties of selective laser-sintered PA12 specimens. Progr Addit Manuf 2025;10:3559–72. https://doi.org/10.1007/s40964-024-00826-3.
[47] Chen K, Teo HWB, Tian Y, Wu S, Kang G, Zhou K, et al. Effect of build direction on tension–tension low cycle fatigue behavior of polyamide 12 parts printed by multi jet fusion. Int J Fatig 2023;170:107514. https://doi.org/10.1016/j.ijfatigue.2023.107514.
[48] Calignano F, Giuffrida F, Galati M. Effect of the build orientation on the mechanical performance of polymeric parts produced by multi jet fusion and selective laser sintering. J Manuf Process 2021;65:271–82. https://doi.org/10.1016/j.jmapro.2021.03.018.
[49] Adach M, Sokołowski P, Piwowarczyk T, Nowak K. Study on geometry, dimensional accuracy and structure of parts produced by multi jet fusion. Materials 2021;14:4510. https://doi.org/10.3390/ma14164510.
[50] D'Andrea D, Crisafulli D, Risitano G, Santonocito D. Rapid fatigue life evaluation over time of PA12 obtained by multijet fusion printing process. Int J Fatig 2025;200:109124. https://doi.org/10.1016/j.ijfatigue.2025.109124.